ACS MATERIALS LETTERS

www.acsmaterialsletters.org

LETTER

High-Speed and High-Resolution 3D Printing of Self-Healing and Ion-Conductive Hydrogels via μCLIP

Wenbo Wang, Siying Liu, Luyang Liu, Saleh Alfarhan, Kailong Jin, and Xiangfan Chen*

Cite This: *ACS Materials Lett.* 2023, 5, 1727–1737

Read Online

ACCESS | Metrics & More | Article Recommendations | Supporting Information

ABSTRACT: Conductive and self-healing (SH) hydrogels have been receiving continuous attention, which could broaden the design of ionotronic devices for health monitoring systems and soft robots with the ability to repair damage autonomously. So far, three-dimensional (3D) fabrication of such SH hydrogels is mainly limited to traditional molding/casting or extrusion-based 3D printing methods, which limits the formation of sophisticated structures with high-resolution features. Furthermore, the need of external stimuli (e.g., water, heat, and pH change) to achieve SH behavior could restrict their wide application. Herein, we report an ion-conductive SH hydrogel suitable for a home-built high-resolution and high-speed 3D printing process, micro continuous liquid interface production (μCLIP). This material system relies on interpenetrating polymer networks (IPN) hydrogel formed by physically cross-linked poly(vinyl alcohol) combined with chemically/ionically cross-linked poly(acrylic acid) and ferric chloride. By carefully optimizing the resin's composition, we can balance high-resolution printability and superb SH capability, at the same time manifesting sufficient ion conductivity. Specifically, complex 3D structures with microscale features (down to 100 μm) can be printed at speeds up to 16.5 μm s^{-1}. Upon damage occurs, hydrogen bonds within hydroxyl and carboxyl groups, as well as ionic bonds generated from ferric ions, contribute together to achieve fast and high efficiency SH, which can restore 90% (100%) of the original mechanical strength at room temperature within 4 h (8 h) without any external stimulus. In addition, both the as-printed and self-healed hydrogels manifest superior ion conductivity and stretchability. Therefore, the SH hydrogels can be rapidly printed and tailored as customized wearable sensors, and the sensing capabilities were quantitatively investigated and compared. In terms of applications, SH hydrogel-based knuckle sensors were prototyped to detect a finger's folding and unfolding motions.

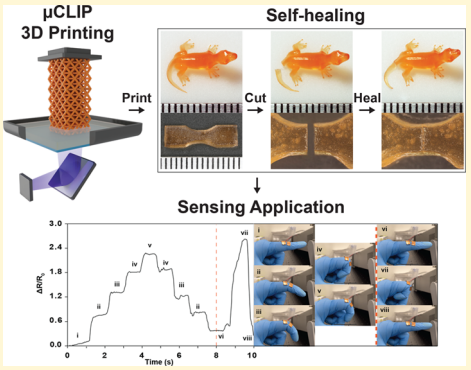

1. INTRODUCTION

Hydrogels are soft materials capable of holding large amounts of water in physically and/or chemically cross-linked three-dimensional (3D) hydrophilic polymer networks.[1−3] They are receiving enormous attention for wide applications, such as drug release, tissue scaffolds, and electronic skin.[4−6] Particularly, 3D hydrogels with ionic conductivity have been explored in ionotronic devices to mimic human skin, which can be directly applied to sense load, deformation, temperature, etc.[7] Benefiting from their high stretchability and fatigue resistance, hydrogels can be applied on complex surfaces for improved performance.[8,9] However, once a crack occurs, the hydrogel's mechanical strength decreases rapidly as the crack propagation leads to irreversible failure.[10] Therefore, the self-healing (SH) ability has been considered to be imparted to extend their lifetime performance for practical applications.[11−13] Till recently, SH hydrogels have been realized via various strategies.[14−17] While some require external stimuli, including changes in pH, temperature, and light, to reassociate polymer chains, others utilize the bonding agents within the material network to achieve SH.

From the manufacturing perspective, SH hydrogel structures are usually fabricated by traditional methods, such as molding or casting, which have limitations for achieving 3D objects with sophisticated structures.[18−21] In contrast, additive manufacturing (AM) technologies, also known as 3D printing, have been explored to directly fabricate customized 3D hydrogel structures.[22−25] Heretofore, 3D SH hydrogels have been commonly fabricated by extrusion-based 3D printing pro-

Received: May 2, 2023
Accepted: May 16, 2023
Published: May 18, 2023

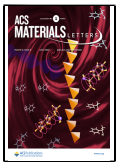

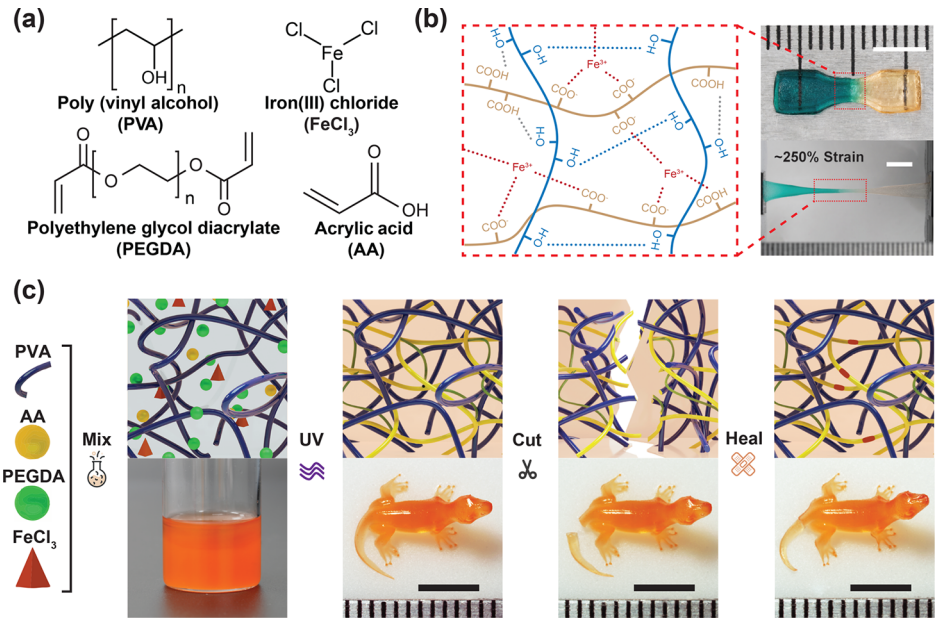

Figure 1. Design concept and preparation of ion-conductive SH hydrogel. (a) Chemical structures of the major components to form the IPN hydrogel. (b) SH mechanism supported by hydrogen bonds formed by hydroxyl groups in PVA, as well as ionic bonds formed between ferric ions and carboxylate ions from PAA. (c) Schematic illustration of the preparation, 3D printing, and SH processes of the hydrogel with a corresponding photo of the 3D printed lizard whose tail was cut and self-healed. Scale bars: 5 mm.

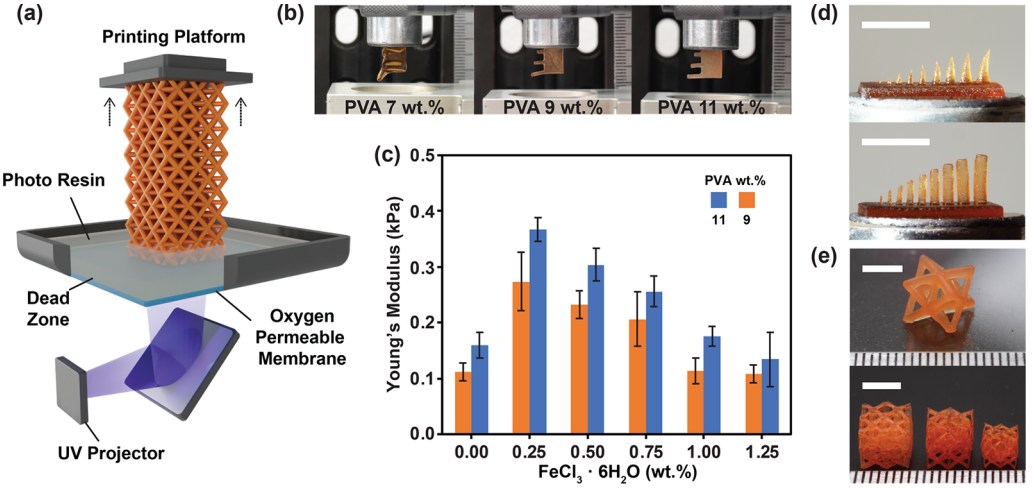

Figure 2. 3D printing via μCLIP. (a) Schematic illustration of the μCLIP system. (b) Optical images of 3D printed overhanging beams with aspect ratios of 2, 3, and 4, using representative resins with 1 wt % $FeCl_3 \cdot 6H_2O$. (c) Comparison of Young's modulus with various concentrations of PVA and $FeCl_3 \cdot 6H_2O$. Error bars represent standard deviation, n = 4 independent replicates. (d) 3D printed needles and pillars with base diameters ranging from 100 to 900 μm incrementally, with an aspect ratio of 4:1. (e) 3D printed multiscale octet truss structures. Scale bars: 5 mm.

cesses, such as direct ink writing (DIW).[26−28] For example, Liu et al. reported using a DIW bioprinter to print hydrogels with SH capability enabled by reassociated chains after being heated above gel−sol temperature.[26] Darabi et al. also reported utilizing DIW to print hydrogel capable of healing autonomously because of hydrogen bonding and ionic interactions.[29] However, those printing techniques are still experiencing challenges, such as resolution, printing speed, structural complexity, and mechanical integrity.[30] In detail, the printing resolution of DIW is typically in the range of hundreds of micrometers.[24] The inherent speed-accuracy trade-off resulting from the point-by-point serial nature significantly constrains the overall scalability in manufacturing 3D parts with fine features.[31] Moreover, due to the relatively low stiffness of the material, the fabrication of overhanging features is challenging without supporting structures.[32,33]

To overcome those challenges, vat photopolymerization (VP) strategies, such as stereolithography (SLA) and digital light processing (DLP), have been reported to fabricate hydrogels with improved geometrical complexities and resolution.[34,35] For example, Caprioli et al. successfully utilized DLP to print 3D hydrogels from poly(vinyl alcohol) and acrylic acid with the SH effect promoted by hydrogen bonds within the interpenetrating networks.[36] However, besides the drawback that the SH efficiency is only 70% and printing resolution is limited to millimeter scale, a continuous high-humidity environment is demanded during the slow DLP printing. It is worth noting that there are remaining difficulties

https://doi.org/10.1021/acsmaterialslett.3c00439
ACS Materials Lett. 2023, 5, 1727−1737

in balancing the SH performance and rapid high-resolution 3D printing. Hydrogels with excellent SH performance typically contain a large water content, which weakens the mechanical strength and makes forming complex self-standing 3D structures challenging.[21,26,37] Furthermore, external stimuli (e.g., water and heat) are required to enhance the SH performance, which limits the applicability.[12,36,38] Therefore, high-resolution 3D printing of efficient autonomous SH hydrogel at high speeds remains challenging.

Herein, we successfully developed a 3D-printable interpenetrating polymer network (IPN) hydrogel system that not only presents distinguished SH efficiency without applying an external stimulus but also manifests satisfactory ionic conductivity for sensing. By incorporating physically cross-linked poly(vinyl alcohol) (PVA) and chemically/ionically cross-linked poly(acrylic acid) (PAA) and ferric chloride ($FeCl_3$) networks, these double networks entangle and interpenetrate each other (Figure 1a). Benefiting from the hydrogen bonds and migration mobility of PVA, paired with the strong ionic bonds between diffused ferric ions (Fe^{3+}) and carboxyl groups ($-COO^-$) in PAA (Figure 1b), the hydrogel is capable of repairing damaged areas autonomously (schematics shown in Figure 1c).[21,37,39] To achieve high-resolution 3D printing of the hydrogel (Figure 1c), a home-built high-speed microcontinuous liquid interface production (μCLIP) system was developed (Figure 2a and Supporting Information Section 3).[40] Compared to most vat-polymerization processes, such as projection micro stereolithography (PμSL) or digital light processing (DLP), μCLIP has the advantage of fabricating sophisticated 3D structures with smooth surface finish and homogeneous mechanical properties at high speeds (up to 16.5 $\mu m \cdot s^{-1}$ in this work). More importantly, the significantly shortened printing time minimizes the impact of dehydration and enables the stable fabrication of functional 3D hydrogels especially those with high water concentration.[41] Through systematic characterizations, we varied the compositions of the resins to achieve a balance across the mechanical properties, printability, and self-healing efficiencies of the IPN hydrogels, which has not been achieved before (Figure S1). Moreover, the home-built μCLIP produced self-healing hydrogel manifested excellent conductivity, which can be tailored as flexible ionotronics, such as wearable sensors. To the best of our knowledge, this work provides the first strategy for rapid 3D printing of high-resolution ($\leq$100 μm) ion-conductive hydrogels equipped with ultrahigh self-healing efficiency without the need for external stimuli.

2. RESULTS AND DISCUSSIONS

2.1. Material System Design. The photocurable resin for 3D printing of the SH hydrogel was prepared by homogeneously mixing PVA aqueous solution with the chemical network precursors, acrylic acid (AA) solution. The AA solution contains AA monomers, poly(ethylene glycol) diacrylate (PEGDA) as chemical cross-linker, ferric chloride ($FeCl_3 \cdot 6H_2O$) as both ionic conductors and physical cross-linker,[42] and (2,4,6-trimethylbenzoyl) phosphine oxide (TPO) as water-soluble photoinitiator (Figure 1a, details in the Supporting Information Section 2). In addition, ferric chloride could also improve printing resolutions benefiting from the strong absorption in the UV range.[43] PVA and PAA were selected to form the IPN hydrogel system because of the high mobility of polymer chains and extensive bond-forming groups (carboxyl and hydroxyl groups).[44,45] Upon physical damage, the PVA chain diffusion across the interface can form new hydrogen bonds not only among its own hydroxyl groups ($-OH$)[39,46,47] but also with the carboxylic groups ($-COOH$) of PAA,[48] hence, contributing to the SH ability (Figure 1b). In previously reported hydrogel systems without the addition of ferric ions (Fe^{3+}), the PVA's concentration needs to be raised to above 15−30 wt % to enable satisfactory SH effect[36,39] which significantly increases the resin's viscosity, consequently leading to failure of high-resolution printing by μCLIP.[49] Alternatively, to improve the SH capabilities without the demand for high PVA concentration, ferric chloride was introduced into the system to form the dynamic ionic bonds between ferric ions and carboxyl groups of PAA in addition to the hydrogen bonds (Figure 1b).[21,50,51] By combining these two-pronged strategies, the SH efficiency can efficiently reach over 90% (both stress and strain) within a reasonable healing time frame (<4 h), even for the resin with PVA's concentration as low as 9 wt %. The SH capability of the 3D printed structures can be visualized by the two printed dumbbell-shaped specimens with/without the addition of methyl blue dye. These two specimens were cut and recontacted together for SH (Figure 1b). After 24 h of SH at room temperature, the blue color diffusion from the dyed half to the other indicates efficient mobility within the IPN, and the healed specimen can withstand stretching over 250% strain before failure. Besides the excellent SH performance, benefiting from the high water concentration (up to 67 wt %) and free ions (Fe^{3+}), the IPN hydrogel also shows ion-conductivity up to $4.76 \times 10^{-1} \pm 2.28 \times 10^{-1}$ S m^{-1}, which is comparable with previously reported strain sensing devices.[51−53] The porous networks benefiting polymer chain and ion migration were confirmed by characterizing the freeze-dried samples with scanning electron microscope (SEM) (Supporting Information Section 4, Figure S5).

2.2. Rapid 3D Printing by Micro-Continuous Liquid Interface Printing (μCLIP). To yield rapid high-resolution 3D printing of the IPN hydrogels, we have developed a home-built micro continuous liquid interface printing (μCLIP) process (Figure 2a), which overcomes limitations associated with traditional SLA or DLP processes, such as long fabrication time scale due to stepwise layer-by-layer curing, stair-stepping roughness caused by delamination and movement, and inhomogeneous printout because of solvent evaporation during the long printing period.[54] Specifically for the hydrogel, a longer printing time will lead to dehydration of the hydrogels, affecting the homogeneity of the printed parts.[36,55] To achieve rapid high-resolution printing, μCLIP uses an oxygen-permeable and optically transparent window to generate a thin polymerization-free zone, referred to as a "dead zone", near the window due to inhibition induced by oxygen molecules.[41] As a result, continuous printing can be realized by allowing the resins to reflow into the printing area simultaneously as the platform moves up. For the μCLIP, the computer-aided design (CAD) models were first sliced into a series of 2D grayscale bitmaps with various slicing layer thicknesses along the printing direction. By further reducing slicing thickness, a smooth surface finish can be achieved.[41] The sliced bitmap patterns were then projected via a UV light engine with desired light intensity onto the window to selectively cure the resin above the "dead zone" into solid structures. Simultaneously, as shown in Video S1, the printing platform was continuously raised upward at the appropriate

https://doi.org/10.1021/acsmaterialslett.3c00439
ACS Materials Lett. 2023, 5, 1727−1737

speed, which was measured and retrieved by using a speed-working curve model (Supporting Information Section 4, Figure S3).

To achieve high-resolution and reliable 3D printing of hydrogels, it is crucial to maintain reasonable mechanical strength, particularly stiffness, to ensure the final printed samples' freestanding structures and shape fidelity. In this IPN hydrogel system, the concentrations of AA and PVA in the hydrogel play a vital role in determining its mechanical strength as they form the backbone network.[44,56] In our study, we found that the capability of shape retention (Figure S6) and the mechanical strength (Figure S12) of the cured hydrogels was significantly improved by increasing AA concentration while keeping PVA's concentration constant. As shown in Figure S6, a minimum of 20 wt % AA is required to construct sufficient self-standing 3D structure with overhanging features, while the printout from resins with AA concentration below 20 wt % showed unrecognizable 3D structures (Figure S6). This indicates that raising chemical cross-linking density can effectively enhance the shape retention capability of the hydrogels. Additionally, the marginally increased viscosity of reins as the incremental AA concentration did not affect printability (Figure S9b) and can be neglected. To optimize the printability and self-healing efficiency, the effect of PVA concentration was further investigated while maintaining the minimum sufficient concentration of AA. It is important to note that as the concentration of PVA rises, the viscosity of the resin also increases in a monotonic manner (Supporting Information Section 5, Figure S9a). The higher viscosity makes the replenishment of fresh resins into the "dead zone" even more challenging.[49] Specifically, when the PVA content is higher than 11 wt %, printings made with μCLIP resulted undercuring or even failure to form complex structures with large cross-section areas (Figure S7).

Furthermore, we systematically characterized the effect of resins' compositions on Young's modulus (Figure 2c) and explored the corresponding printability as well as the shape retention performance indicated by printed overhanging structures (Figure 2b). In detail, dumbbell-shaped samples (Supporting Information Section 6, Figure S11) were printed from resins with various concentrations of PVA (9 and 11 wt %) and $FeCl_3{\cdot}6H_2O$ (0.00−1.25 wt %) by μCLIP under appropriate parameters retrieved from the speed-working curve. Then the tensile tests were performed by a customized mechanical tester (details in Supporting Information Section 6 and Video 2), and Young's modulus was then calculated by taking the gradient of the stress−strain curves up to the fracture point[57] (details in Supporting Information Section 6). Through tests, we found that resin with PVA concentration up to 11 wt % still enabled the rapid printing on μCLIP though it manifested the increasing viscosity. Likewise, a study was also conducted to determine the concentration of ferric chloride, as the significant ionic cross-linker was reported to contribute the consequential amount of effects on self-healing performance.[37] As shown in Figure 2c, Young's modulus of the hydrogel increased gradually with the rise of PVA concentration from 9 to 11 wt %. Specifically, in the case without ferric chloride (0.00 wt % $FeCl_3{\cdot}6H_2O$), Young's modulus of the hydrogel increased from 0.11 to 0.16 kPa, which confirms that the backbone network and hydrogen bonds produced by PVA have a significant effect on the mechanical strength of the hydrogel.[58] Upon adding 0.25 wt % $FeCl_3{\cdot}6H_2O$ into the hydrogel material, a significant improvement was observed in Young's modulus. This enhancement was attributed to a synergistic effect resulting from the crack bridging provided by the covalent cross-linking network, as well as hysteresis achieved through unzipping the ionic cross-linking network.[59] However, by further increasing the concentration of ferric chloride in the system, Young's modulus of the 3D printed hydrogel decreased gradually. This is due to the reduced cross-linking density resulting from the intense UV absorption of ferric chloride, which is consistent with the photorheology measurements (lower plateau modulus after photocuring in Figure S10). Given the strong absorption of UV light by ferric chloride, we determined that a concentration of 1.25 wt % was the upper limit that could provide sufficient irradiation penetration depth to facilitate acceptable printing speed and curing depth of μCLIP.

To optimize the resins' capability of shape retention, rationally designed structures consisting of overhanging beams with an aspect ratio of 2, 3, and 4, respectively, were printed from resins previously tested (representative printout examples are shown in Figure 2b, and other examples are shown in Supporting Information Section 4, Figure S6−S8). For example, the printed hydrogels using resins containing 9 or 11 wt % PVA show satisfactory shape retention (defined as good shape retention in Table 1 and Table 2), making the fabrication of complex 3D structures possible. In contrast, the counterpart printed from resins containing 7 wt % PVA showed unsatisfied deformations during and after the printing (defined as poor shape retention in Table 1). Besides printability, printing resolution is another important criterion, which can be evaluated vertically and laterally. The vertical resolution was determined as the curing depth (*Cd*), which ensures precise polymerization thickness. Resin compositions that can achieve the desired *Cd* to match the slicing layer thickness of 5 μm with appropriate printing parameters were classified as acceptable resolution vertically. The printing parameters for each resin composition were determined using a speed-working curve. (Supporting Information Section 4, Figure S3).[41,60] It was found that resin with the concentration of $FeCl_3{\cdot}6H_2O$ being 0.50 wt % or less failed to produce 3D structures with recognizable features due to thicker optical absorption depth (Table 1).[61] Based on the characterization results, different combinations of PVA (9−11 wt %), $FeCl_3{\cdot}$

Table 1. Shape Retention Capability, and Printing Resolution of Hydrogels with Various Compositions[a]

		$FeCl_3{\cdot}6H_2O$ (wt %)					
		0.00	0.25	0.50	0.75	1.00	1.25
PVA (wt %)	7	↓, □	↓, □	↓, □	↓, ■	↓, ■	↓, ■
	9	↑, □	↑, □	↑, □	↑, ■*	↑, ■*	↓, ■
	11	↑, □	↑, □	↑, □	↑, ■*	↑, ■*	↑, ■*

[a]Shape retention: ↑, good; ↓, poor; printing resolution: ■, acceptable; □, unacceptable; *, preferred.

Table 2. Shape Retention Capability and Printing Resolution of Hydrogels with Various AA[a]

		AA (wt %)				
		10	15	20	25	30
PVA (wt %)	11	↓, □	↓, □	↑, ■*	↑, ■*	↑, ■*

[a]Shape retention: ↑, good; ↓, poor; printing resolution: ■, acceptable; □, unacceptable; *, preferred.

https://doi.org/10.1021/acsmaterialslett.3c00439
ACS Materials Lett. 2023, 5, 1727−1737

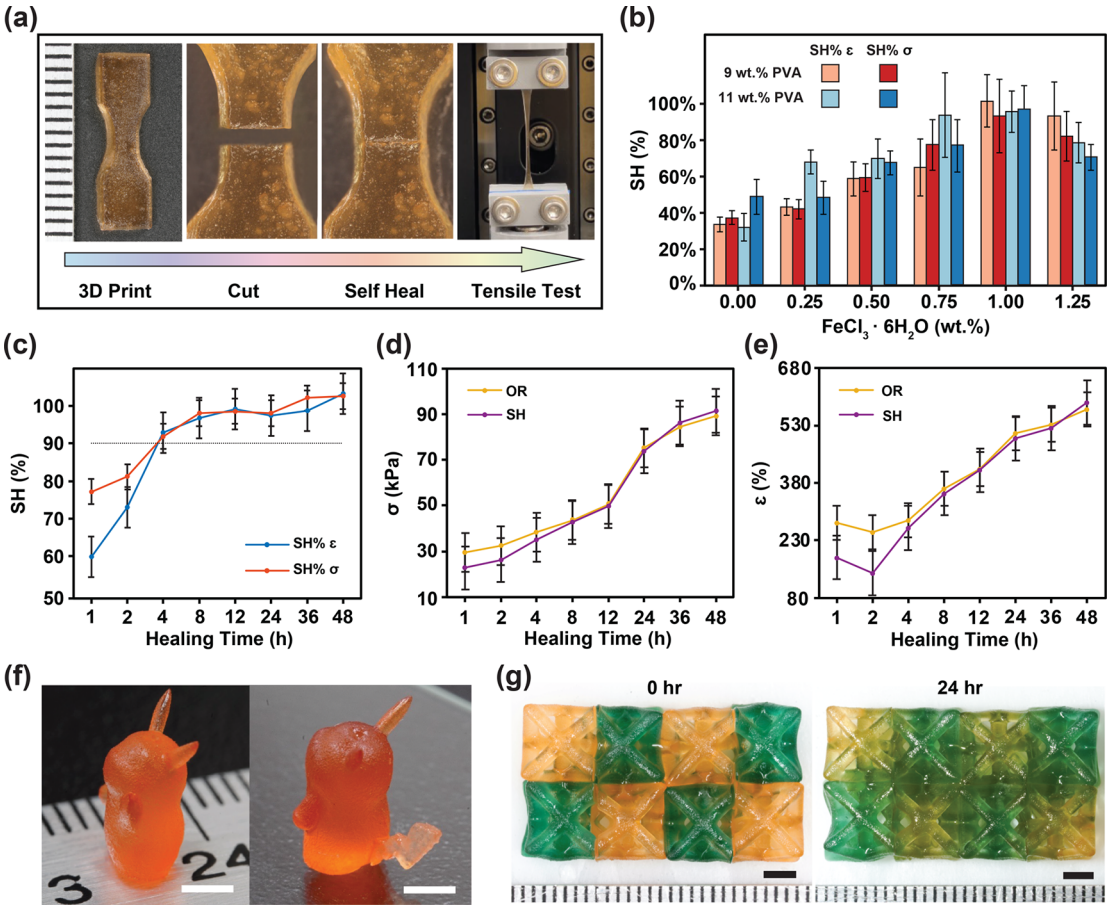

Figure 3. Characterization of SH properties of the 3D printed hydrogels. (a) Schematics of characterization of SH efficiency. 3D printed dumbbell-shaped samples were cut in the middle and then reattached together to be stored in a sealed environment for later tensile tests. (b) Comparison of SH efficiency of the hydrogels with increasing content of $FeCl_3$·$6H_2O$, and PVA concentrations of 9 and 11 wt %. (c) SH efficiencies of the hydrogels for various healing times. (d) The ultimate tensile stress and (e) elongation at break of SH and original samples with various healing times. Error bars represent standard deviation, n = 6 independent replicates. (f) 3D printed solid Pikachu with SH tail as "print-and-joint". (g) SH cuboid assembled with octet truss units printed from resins with/without methylene blue (individual units are shown in Figure S16). Scale bars: 3 mm.

$6H_2O$ (0.75−1.25 wt %), and AA (20−30 wt %) were selected for the following printing characterization. As an example to achieve optimal vertical resolution, the corresponding printing speed V_s of ∼16.5 μm s^{-1} (or ∼13 μm s^{-1}) was selected for a representative resin containing 11 wt % PVA and 1 wt % $FeCl_3$·$6H_2O$ (or 11 wt % PVA and 1.25 wt % $FeCl_3$·$6H_2O$). This high speed enables the fabrication of 10 mm-height complex structures in just ∼10 min, which is significantly faster than the 12 h printing process with the PμSL system in our previously reported work.[62] Moreover, the theoretical lateral resolution for our μCLIP system was determined to be 7.6 × 7.6 μm/pixel based on the optical projection system. During the printing process, features comprising multiple pixels can be retained. To experimentally explore the printable limit of feature sizes, a series of microscale features, e.g., dots, were printed and measured (Supporting Information Section 4, Figure S4). The resins that successfully produced dots with desired dimensions (smallest feature = 100 μm) (error ≤5%) were determined to be resolution-acceptable in Table 1 and Table 2. To further demonstrate the 3D printing resolution, we performed a series of tests using structures composed of arrays of rods and needles with a high aspect ratio of 4:1 and base diameters ranging from 100 to 900 μm (Figure 2d). This range of base diameters is particularly significant, as it covers a wide range of potential applications, from the creation of small-scale biomedical devices to the development of complex microelectronic components. In addition to these tests, we also used μCLIP to demonstrate the printability of the representative SH hydrogel resin. This allowed us to create various complex 3D structures, such as octet truss lattice structures with overhanging components of varying dimensions, including beam diameters ranging from 150 μm to 1 mm (Figure 2e). Taken together our findings confirmed the capability of the technology to rapidly fabricate high-resolution, intricate 3D structures with great accuracy and precision. These results are significant because they indicate that this strategy can be applied to a wide range of fields, including microscale devices, tissue engineering, and advanced electronics to create complex structures with high resolution and fidelity (Video S1).

2.3. Characterization of SH Hydrogels. The self-healing (SH) capability of the 3D printed hydrogel was quantitatively characterized by performing tensile tests on the as-printed and self-healed dumbbell-shaped samples. As illustrated in Figure 3a, batches of samples were printed from different resin compositions with corresponding optimal printing parameters (i.e., printing speed and light intensity) according to the speed working curve (Figure S3c). For each batch, half of the samples were cut in the middle, reattached together manually

https://doi.org/10.1021/acsmaterialslett.3c00439
ACS Materials Lett. 2023, 5, 1727−1737

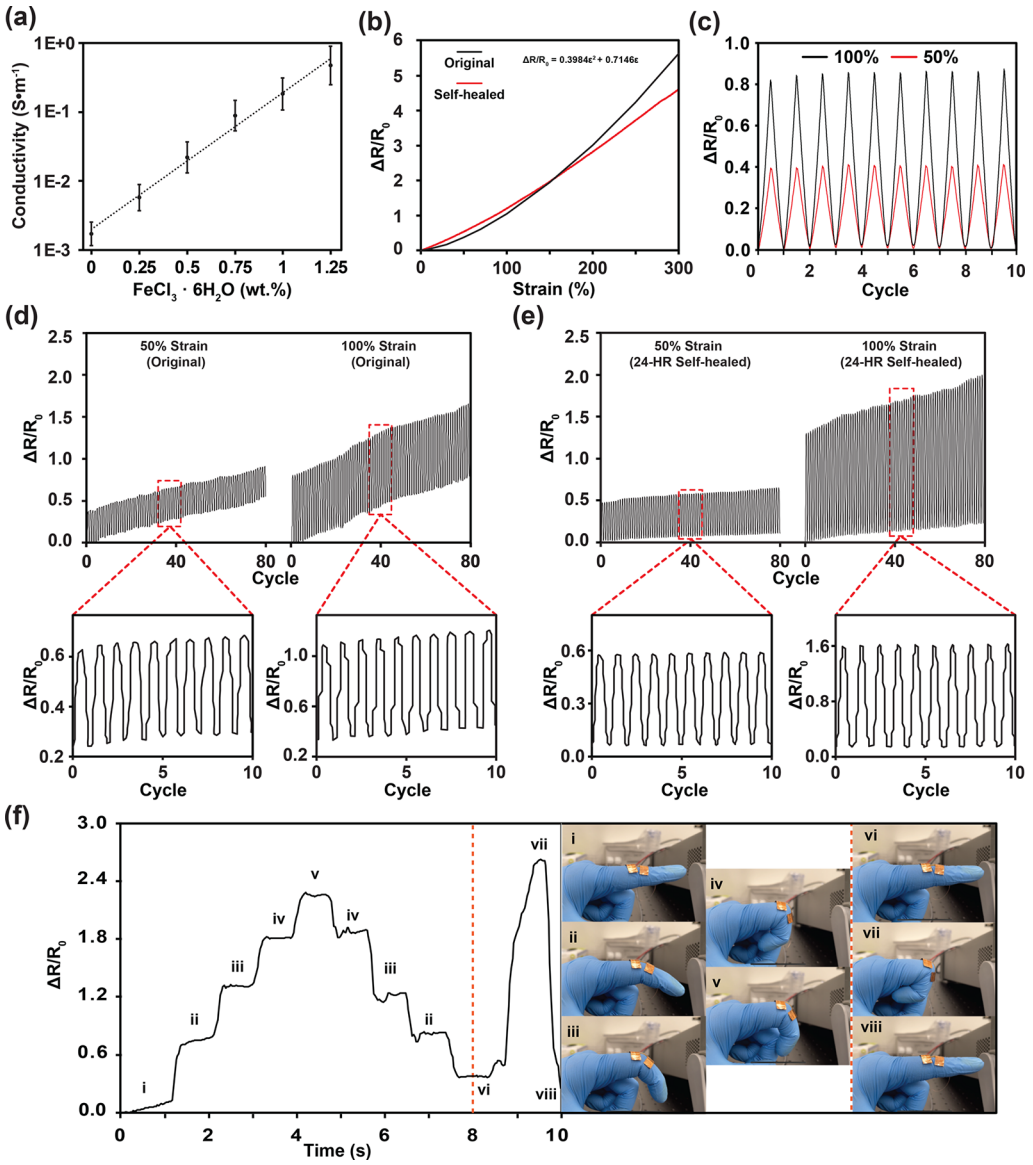

Figure 4. Characterization of ion conductivity and sensing performance of tensile strain. (a) Measured conductivity of 3D printed SH hydrogel with different concentrations of $FeCl_3$·$6H_2O$. (b) Relative resistance change ($\Delta R/R_0$) of as-printed and 24-h self-healed samples versus tensile strain. (c) Measured resistance change with 50% and 100% strain over 10 cycles with the original 3D printed sensor. Strain rate: 20 mm·s^{-1}. (d, e) Cyclic stability measurement of (d) as-printed and (e) self-healed sensors of 80 cycles with strain up to 50% (or 100%). Strain rate: 50 mm s^{-1}. (f) 3D printed wearable hydrogel sensor to detect a finger's folding and unfolding motions at various bending angles.

within a short time, and then healed autonomously in a sealed environment without any external stimuli, which are termed as self-healed samples hereafter for simplification. It is worth mentioning that each batch, including self-healed and as-printed samples, was sealed in the same container for the same time to maintain the identical storage condition to minimize the influence from dehydration. Once the specific time had been reached for each batch, tensile tests were performed on self-healed and as-printed samples to evaluate the SH efficiency. The SH efficiency is defined in terms of the ratios of mechanical strength of self-healed samples over the as-printed samples, of which elongation at break (ε) and ultimate tensile stress (σ) was utilized,[36,63,64] as expressed below:

$$\mathrm{SH}\%(\varepsilon) = \varepsilon_{\text{self-healed}}/\varepsilon_{\text{as-printed}} \quad (1)$$

$$\mathrm{SH}\%(\sigma) = \sigma_{\text{self-healed}}/\sigma_{\text{as-printed}} \quad (2)$$

We first explored the effect of hydrogen bonds and ionic bonds on SH performance by evaluating the SH efficiency of dumbbell-shaped samples printed from resins with PVA concentrations of 9 and 11 wt % paired with various concentrations of $FeCl_3$·$6H_2O$ (0−1.25 wt %) (Table S1). The SH efficiencies (SH%(ε) and SH%(σ)) for the printed hydrogels after 24 h of healing were measured and calculated according to the aforementioned protocols. As shown in Figure 3b, without the presence of ferric chloride (0 wt % $FeCl_3$·$6H_2O$), the SH efficiencies of the printed hydrogels are all lower than 50% regardless of whether the PVA's concentration is 9 or 11 wt %, which means these hydrogels can only restore less than half of the original strength. As the $FeCl_3$·$6H_2O$ concentration increased incrementally to 1 wt %, the SH

https://doi.org/10.1021/acsmaterialslett.3c00439
ACS Materials Lett. 2023, 5, 1727−1737

performance was gradually improved up to 100%, and the printed hydrogels can achieve full restoration in mechanical strength with 1 wt % $FeCl_3{\cdot}6H_2O$. This phenomenon indicates the strong effect on SH supported by the ionic bonding provided by ferric ions. However, it was also found that the SH efficiency tends to decrease when the concentration of $FeCl_3{\cdot}6H_2O$ increases to 1.25 wt %. This could be possible due to the excess ferric chloride acting as UV absorbers, which significantly suppressed the photoinitiation, thus resulting in a lower polymerization rate and fewer PAA chains during 3D printing. On the other hand, the SH efficiency did not exhibit a significant difference between hydrogels with different PVA concentrations (9 and 11 wt %) at the same level of ferric chloride, which could possibly be a result of saturated hydrogen bonds and PVA migration within the IPN. In addition, to investigate the effect of AA concentration on SH performance, SH tests were also performed on hydrogels prepared by resins containing AA concentration from 20 wt % to 30 wt % while maintaining 11 wt % PVA (Table S1). It was found that the SH performance decreased significantly from ∼100% (SH%(σ) and SH%(ε)) to ∼45% (SH%(σ)) and 40% (SH%(ε)) (Figure S14). This phenomenon can be attributed to the reduced mobility of ferric ions and hydrogen migration within the denser network introduced by higher chemical cross-linking density.[65] Although increasing cross-linking density effectively improves the printability of the resin, the minimum required AA concentration of 20 wt % was selected to balance SH efficiency, 3D forming, and mechanical strength of the hydrogel synergistically, along with 1 wt % $FeCl_3{\cdot}6H_2O$ and 11 wt % PVA as representative feedstock for μCLIP and later studies.

To explore the time dependence of the SH efficiency of the 3D printed hydrogel, various healing time from 1 to 48 h was applied to the cut samples to restore their mechanical strength (details in Supporting Information Section 7, Figure S15). As shown in Figure 3c, the printed hydrogel specimen from selected resin exhibited a high-efficiency SH after healing for 4 h, restoring over 90% of its mechanical strength, which indicates that the hydrogel can achieve a high SH efficiency in a short time without needing any external stimulus. Though there are some 3D printable SH hydrogels being reported, most of them still require tens of hours to days to autonomously restore the mechanical strength,[66,67] and some others should demand external stimulus including water and heat to achieve satisfied SH performance.[26,36] Moreover, after healing for 8 h, it approached full restoration in terms of ultimate stress and elongation at break, and maintained steady improvement for longer durations (Figure 3c). It is worth noting that the ultimate stress and elongation at break of both as-printed and self-healed samples at different storage times gradually increased, which is mainly caused by the slow dehydration of the samples (Figure 3d, e). Therefore, storing the self-healed samples and original samples in the same sealed environment for the same time is essential to obtain a valid comparison, with ambient conditions being consistent. To visualize the SH, we printed a series of 3D structures with the optimal resin composition and processing parameters. For example, as shown in Figure 3f, a Pikachu and its long tail were printed separately by μCLIP, then attached together, and self-healed for 4 h by taking advantage of the superior SH capability. This provides an alternative approach, termed as "print-and-joint", to produce sophisticated structures containing large overhanging features rather than through adding supporting structures. As illustrated in Figure 3g, a series of octet truss units were printed (Figure S16) using resin with and without methylene blue and were assembled together in cross combination to form into a single part. The significant color diffusion further indicates sufficient mobility within the porous IPN. Consequently, we demonstrate the capability of postassembly of 3D printed hydrogels by taking advantage of the SH feature, which could provide potential opportunities for reconfigurable soft robot.[68,69]

2.4. Electrical and Piezoresistive Properties of 3D Printed SH Strain Sensors. Benefiting from a large amount of water (∼67 wt %) and mobility of free ions (i.e., Fe^{3+}, Cl^-), the 3D printed SH hydrogel also shows satisfactory ion conductivity.[70,71] The conductivity of the printed hydrogel with varying concentrations of ferric chloride was first measured by a home-built characterization setup (details in Supporting Information Section 8 and Supporting Information Section 8, Figure S17). At different ferric chloride concentrations, the resistance of a series of specimens with varying thicknesses was measured to retrieve the conductivity (details in Supporting Information Section 8, Figure S18). In detail, the samples without ferric chloride manifest a conductivity of $1.69 \times 10^{-3} \pm 8.14 \times 10^{-4}$ S m^{-1}, which is mainly originated from carboxyl groups (−COOH) within PAA.[72] By raising $FeCl_3{\cdot}6H_2O$ concentration up to 1.25 wt %, the conductivity approximately linearly increases up to $4.76 \times 10^{-1} \pm 2.28 \times 10^{-1}$ S·m^{-1} (Figure 4a), which is about three magnitudes higher than those without ferric chloride. More importantly, this conductivity is comparable with the state-of-the-art ion conductive hydrogels.[73] To visually demonstrate the ion-conductivity, 3D printed hydrogel was utilized to compose a circuit to provide power for a LED (Video S3). These results further supported our hypothesis that the free ions introduced by the ferric chloride contribute the most and can significantly improve the conductivity.

Strain sensing using the conductive hydrogel can be accomplished by measuring the change in resistance of the hydrogel in response to applied mechanical strain or deformation. When the hydrogel is subjected to mechanical strain, its dimensions and surface area changes, which can alter the electrical properties of the material, such as its resistance to the flow of electrical current.[74] To validate the feasibility of applying the hydrogel for sensing applications, piezoresistive properties, the relative resistance change ($\Delta R/R_0$) in response to mechanical strain(ε) variation of the printed samples was characterized using a motorized stage (details in Supporting Information Section 8) and a coupled multimeter. The hydrogel's relative resistance ($\Delta R/R_0$) was formulated as $\Delta R/R_0 = (R - R_0)/R_0$, where − is the resistance after uniaxial stretching and R_0 is the resistance before stretching. The mechanical strain (ε) was calculated as $\varepsilon = (l - l_0)/l_0$, where l is the hydrogel's length after stretching and l_0 is the length before stretching (Figure 4b). In addition, the relative resistance changes versus strains of the strain sensor can be fit into a parabolic equation $\Delta R/R_0 = 0.3984\varepsilon^2 + 0.7146\varepsilon$.[75] As the strain increased from 0% to 300% with the rate of 1 mm s^{-1}, the relative resistance increased significantly and steadily up to 5.59 and 4.56 for the as-printed and self-healed hydrogels, respectively (Figure 4). It is worth mentioning that there is no distinct signal decaying for the self-healed specimens compared with the as-printed ones, confirming the applicability of the ion-conductive hydrogel as strain sensors even after cut and healing. Cyclic tensile loadings with the

https://doi.org/10.1021/acsmaterialslett.3c00439
ACS Materials Lett. 2023, 5, 1727−1737

strain of 50% and 100% were applied to the hydrogel to evaluate the sensing behavior. High repeatability of relative resistance response was observed, and a gradually increased magnitude of response was demonstrated when tensile strain increased (Figure 4c). Furthermore, to better assess the long-term stability of the resistance response with mechanical cycling, the sensors, including as-printed (Figure 4d) and self-healed sensors (Figure 4e), were stretched 80 times with strain up to 50% and 100% at a strain rate of 50 mm s^{-1}. Though there is a gradual upward trend of the relative resistance due to the slow dehydration of the hydrogel over the long cyclic stretching, the resistance response, especially the peak-to-peak amplitude (A_{pp}), is reasonably stable throughout the long-cyclic test. Ongoing studies are being conducted to reduce the dehydration of the SH hydrogel.

Benefiting from optimized printability, excellent tensile elongation, and stable piezoresistivity before and after self-healing, customized wearable strain sensors were rapidly printed from the hydrogel via μCLIP. The sensors were applied to the finger joint to detect the folding motion of the forefinger to demonstrate its feasibility (Figure 4f and Video S4). With both ends being fixed on the finger, the hydrogel sensor is subject to being stretched to corresponding strain when the forefinger is folded. It can be seen that the relative resistance change ($\Delta R/R_0$) of the strain sensor can be reflected in levels corresponding to various bending angles (θ from 0° to 90° as shown in Figure 4f, i–v). In particular, the relative resistance immediately rebounded as the finger returned from full bending (Figure 4f, vii) to full relaxation (Figure 4f, viii) of the sensor. This confirms that the 3D printed SH ion-conductive hydrogel can respond to deformation rapidly as stretchable electronic skin.

3. DISCUSSION

In summary, we have developed a photocurable hydrogel system that not only shows outstanding self-healing performance without the need for external stimulus but also possesses ion conductivity and piezoresistivity for wearable sensing applications. More importantly, we have systematically studied the printability and developed a high-resolution and high-speed 3D printing strategy for printing this hydrogel via μCLIP. In the hydrogel system, interpenetrating networks were realized by combining chemically and ionically cross-linked PAA/Fe^{3+} with robust physically cross-linked PVA chains. The sufficient chain and ion migration within the porous network enables promising SH performance. Upon damage, the hydrogel can restore its mechanical strength from the new physical bonds formed by the hydroxyl and the carboxyl groups within PVA and PAA, as well as ionic bonds generated between the ferric ions and the carboxyl groups from PAA. The cut hydrogel could autonomously recover over 90% of its original mechanical strength after healing for 4 h and achieve complete self-healing after 8 h. This strategy overcame the challenges in 3D printing of PVA hydrogels that typically originated from the trade-off between the requirement of reducing viscosity for resin replenishment and the necessity of high PVA concentration to enable healing capability. For future work, we are currently working on optimizing resin compositions and exploring additional approaches, such as utilizing solvent exchange to partially replace water with glycerol,[76] to mitigate the effects of hydrogel dehydration. These μCLIP printed high-resolution conductive hydrogels offer superior advantages over traditional methods, enabling the creation of complex and customized structures. These hydrogels have the potential for rapid, high-resolution 3D fabrication with self-healing capabilities, making them ideal for constructing patient-specific artificial implants and tissues that are intrinsically 3D with extended lifetime.

■ ASSOCIATED CONTENT

Supporting Information

The Supporting Information is available free of charge at https://pubs.acs.org/doi/10.1021/acsmaterialslett.3c00439.

Section 1, comparison between this work with similar works; Section 2, materials and preparation of photopolymerizable resins; Section 3, home-built μCLIP 3D printing system; Section 4, characterization of 3D printing with μCLIP; Section 5, rheological characterization of photocurable resins; Section 6, characterization of mechanical properties; Section 7, characterization of self-healing performance; Section 8, characterization of electrical and piezoresistive properties; Figure S1, comparison between this work with similar works; Figure S2, CAD of the home-built μCLIP system; Figure S3, characterization of speed working curve model; Figure S4, representative μCLIP produced dots for lateral resolution characterization; Figure S5, SEM image of freeze-dried 3D printed sample; Figures S6–S8, μCLIP produced overhanging structures; Figure S9, viscosity-shear rate curves of resins with various PVA and AA content; Figure S10, photorheological measurements of resins; Figure S11, characterization of mechanical properties of printed hydrogels; Figure S12, Young's modulus of hydrogels prepared using resins with various AA content (PVA 11 wt %); Figure S13, effect of ferric chloride to AA ratio on Young's modulus; Figure S14, self-healing efficiency (24 h) of hydrogels prepared using resin with various AA content (PVA 11 wt %); Figure S15, stress–strain curves of original (solid lines) and SH (dashed lines) 3D printed dumbbell-shaped samples after various storage times; Figure S16, as-printed octet truss units using resin with and without methylene blue; Figure S17, schematic Illustration of the customized two-wire resistance measurement; Figure S18, resistance measurement of samples printed from resins with varying FeCl3 concentrations; Table S1, material composition of the resins tested in the study (PDF)

Video S1, rapid 3D printing via μCLIP (MP4)

Video S2, tensile tests of SH hydrogel (MP4)

Video S3, ion-conductive hydrogel composed circuit (MP4)

Video S4, finger folding sensing (MP4)

■ AUTHOR INFORMATION

Corresponding Author

Xiangfan Chen − *School of Manufacturing Systems and Networks, Arizona State University, Mesa, Arizona 85212, United States;* orcid.org/0000-0002-5627-7530; Email: Xiangfan.Chen@asu.edu

Authors

Wenbo Wang − *School of Manufacturing Systems and Networks, Arizona State University, Mesa, Arizona 85212, United States*

https://doi.org/10.1021/acsmaterialslett.3c00439
ACS Materials Lett. 2023, 5, 1727–1737

Siying Liu − *School of Manufacturing Systems and Networks, Arizona State University, Mesa, Arizona 85212, United States; School for Engineering of Matter, Transport & Energy, Arizona State University, Tempe, Arizona 85287, United States;* orcid.org/0000-0001-7399-5588
Luyang Liu − *School of Manufacturing Systems and Networks, Arizona State University, Mesa, Arizona 85212, United States;* orcid.org/0000-0003-1156-1594
Saleh Alfarhan − *School for Engineering of Matter, Transport & Energy, Arizona State University, Tempe, Arizona 85287, United States;* orcid.org/0009-0005-2629-5948
Kailong Jin − *School for Engineering of Matter, Transport & Energy, Arizona State University, Tempe, Arizona 85287, United States;* orcid.org/0000-0001-5428-3227

Complete contact information is available at: https://pubs.acs.org/10.1021/acsmaterialslett.3c00439

Author Contributions

X.C. conceived the idea and supervised the research. W.W., S.L., L.L., and S.A. conducted the experiments. W.W. and X.C. prepared the manuscript. All authors contributed to the data analysis and manuscript revision and approved the submission. CRediT: **Wenbo Wang** conceptualization, formal analysis, investigation, validation, visualization, writing-original draft, writing-review & editing; **Siying Liu** formal analysis, investigation, methodology; **Luyang Liu** formal analysis, investigation; **Saleh Alfarhan** investigation; **Kailong Jin** supervision, writing-review & editing; **Xiangfan Chen** conceptualization, data curation, formal analysis, funding acquisition, investigation, project administration, resources, supervision, validation, writing-original draft, writing-review & editing.

Funding

This work is funded by Arizona State University (ASU) startup funding, the 2022 Mayo Clinic and Arizona State University (ASU) Alliance for Health Care Collaborative Research Seed Grant Program, and National Science Foundation (NSF) Future Manufacturing (FM) Award (CMMI 2229279).

Notes

The authors declare no competing financial interest.

■ ACKNOWLEDGMENTS

The authors would like to thank Prof. Timothy Long and the Biodesign Center of Sustainable Macromolecular Materials and Manufacturing for providing equipment for photorheology tests.

■ ABBREVIATIONS

3D, 3-dimensional; SH, self-healing; AM, additive manufacturing; DIW, direct ink writing; SLA, stereolithography; DLP, digital light processing; PVA, poly(vinyl alcohol); PAA, poly(acrylic acid); μCLIP, microcontinuous liquid interface production; PμSL, projection micro stereolithography; AA, acrylic acid; PEGDA, poly(ethylene glycol) diacrylate; TPO, (2,4,6-trimethylbenzoyl) phosphine oxide

■ REFERENCES

(1) Nakayama, A.; Kakugo, A.; Gong, J. P.; Osada, Y.; Takai, M.; Erata, T.; Kawano, S. High Mechanical Strength Double-Network Hydrogel with Bacterial Cellulose. *Adv. Funct. Mater.* **2004**, *14*, 1124−1128.
(2) Ahmed, E. M. Hydrogel: Preparation, Characterization, and Applications: A Review. *J. Adv. Res.* **2015**, *6*, 105−121.
(3) Truby, R. L.; Lewis, J. A. Printing Soft Matter in Three Dimensions. *Nature* **2016**, *540*, 371−378.
(4) Ashley, G. W.; Henise, J.; Reid, R.; Santi, D. V. Hydrogel Drug Delivery System with Predictable and Tunable Drug Release and Degradation Rates. *Proc. Natl. Acad. Sci. U. S. A.* **2013**, *110*, 2318−2323.
(5) Jiang, S.; Liu, S.; Feng, W. PVA Hydrogel Properties for Biomedical Application. *J. Mech. Behav. Biomed. Mater.* **2011**, *4*, 1228−1233.
(6) Hu, C.; Zhang, Y.; Wang, X.; Xing, L.; Shi, L.; Ran, R. Stable, Strain-Sensitive Conductive Hydrogel with Antifreezing Capability, Remoldability, and Reusability. *ACS Appl. Mater. Interfaces* **2018**, *10*, 44000−44010.
(7) Yang, C.; Suo, Z. Hydrogel Ionotronics. *Nat. Rev. Mater.* **2018**, *3*, 125−142.
(8) Lin, S.; Yuk, H.; Zhang, T.; Parada, G. A.; Koo, H.; Yu, C.; Zhao, X. Stretchable Hydrogel Electronics and Devices. *Adv. Mater.* **2016**, *28*, 4497−4505.
(9) Liu, X.; Liu, J.; Lin, S.; Zhao, X. Hydrogel Machines. *Mater. Today* **2020**, *36*, 102−124.
(10) Zhang, W.; Hu, J.; Tang, J.; Wang, Z.; Wang, J.; Lu, T.; Suo, Z. Fracture Toughness and Fatigue Threshold of Tough Hydrogels. *ACS Macro Lett.* **2019**, *8*, 17−23.
(11) Deng, Z.; Wang, H.; Ma, P. X.; Guo, B. Self-Healing Conductive Hydrogels: Preparation, Properties and Applications. *Nanoscale* **2020**, *12*, 1224−1246.
(12) Tseng, T.-C.; Tao, L.; Hsieh, F.-Y.; Wei, Y.; Chiu, I.-M.; Hsu, S. An Injectable, Self-Healing Hydrogel to Repair the Central Nervous System. *Adv. Mater.* **2015**, *27*, 3518−3524.
(13) Talebian, S.; Mehrali, M.; Taebnia, N.; Pennisi, C. P.; Kadumudi, F. B.; Foroughi, J.; Hasany, M.; Nikkhah, M.; Akbari, M.; Orive, G.; Dolatshahi-Pirouz, A. Self-Healing Hydrogels: The Next Paradigm Shift in Tissue Engineering? *Adv. Sci.* **2019**, *6*, 1801664.
(14) Kurt, B.; Gulyuz, U.; Demir, D. D.; Okay, O. High-Strength Semi-Crystalline Hydrogels with Self-Healing and Shape Memory Functions. *Eur. Polym. J.* **2016**, *81*, 12−23.
(15) Shi, D.; Liu, R.; Dong, W.; Li, X.; Zhang, H.; Chen, M.; Akashi, M. PH-Dependent and Self-Healing Properties of Mussel Modified Poly(Vinyl Alcohol) Hydrogels in a Metal-Free Environment. *RSC Adv.* **2015**, *5*, 82252−82258.
(16) Burnworth, M.; Tang, L.; Kumpfer, J. R.; Duncan, A. J.; Beyer, F. L.; Fiore, G. L.; Rowan, S. J.; Weder, C. Optically Healable Supramolecular Polymers. *Nature* **2011**, *472* (7343), 334−337.
(17) Taylor, D. L.; in het Panhuis, M. Self-Healing Hydrogels. *Adv. Mater.* **2016**, *28*, 9060−9093.
(18) Hollister, S. J. Porous Scaffold Design for Tissue Engineering. *Nat. Mater.* **2005**, *4*, 518−524.
(19) Yang, L.; Shridhar, S. V.; Gerwitz, M.; Soman, P. An in Vitro Vascular Chip Using 3D Printing-Enabled Hydrogel Casting. *Biofabrication* **2016**, *8*, 035015.
(20) Hou, S.; Ma, P. X. Stimuli-Responsive Supramolecular Hydrogels with High Extensibility and Fast Self-Healing via Precoordinated Mussel-Inspired Chemistry. *Chem. Mater.* **2015**, *27*, 7627−7635.
(21) Shin, S.-H.; Lee, W.; Kim, S.-M.; Lee, M.; Koo, J. M.; Hwang, S. Y.; Oh, D. X.; Park, J. Ion-Conductive Self-Healing Hydrogels Based on an Interpenetrating Polymer Network for a Multimodal Sensor. *Chem. Eng. J.* **2019**, *371*, 452−460.
(22) Hong, S.; Sycks, D.; Chan, H. F.; Lin, S.; Lopez, G. P.; Guilak, F.; Leong, K. W.; Zhao, X. 3D Printing of Highly Stretchable and Tough Hydrogels into Complex, Cellularized Structures. *Adv. Mater.* **2015**, *27*, 4035−4040.
(23) Liu, X.; Yuk, H.; Lin, S.; Parada, G. A.; Tang, T.-C.; Tham, E.; de la Fuente-Nunez, C.; Lu, T. K.; Zhao, X. 3D Printing of Living Responsive Materials and Devices. *Adv. Mater.* **2018**, *30*, 1704821.

(24) Li, J.; Wu, C.; Chu, P. K.; Gelinsky, M. 3D Printing of Hydrogels: Rational Design Strategies and Emerging Biomedical Applications. *Mater. Sci. Eng. R Rep.* **2020**, *140*, 100543.
(25) Blaiszik, B. J.; Kramer, S. L. B.; Olugebefola, S. C.; Moore, J. S.; Sottos, N. R.; White, S. R. Self-Healing Polymers and Composites. *Annu. Rev. Mater. Res.* **2010**, *40*, 179−211.
(26) Liu, S.; Li, L. Ultrastretchable and Self-Healing Double-Network Hydrogel for 3D Printing and Strain Sensor. *ACS Appl. Mater. Interfaces* **2017**, *9*, 26429−26437.
(27) Highley, C. B.; Rodell, C. B.; Burdick, J. A. Direct 3D Printing of Shear-Thinning Hydrogels into Self-Healing Hydrogels. *Adv. Mater.* **2015**, *27*, 5075−5079.
(28) Kuang, X.; Chen, K.; Dunn, C. K.; Wu, J.; Li, V. C. F.; Qi, H. J. 3D Printing of Highly Stretchable, Shape-Memory, and Self-Healing Elastomer toward Novel 4D Printing. *ACS Appl. Mater. Interfaces* **2018**, *10*, 7381−7388.
(29) Darabi, M. A.; Khosrozadeh, A.; Mbeleck, R.; Liu, Y.; Chang, Q.; Jiang, J.; Cai, J.; Wang, Q.; Luo, G.; Xing, M. Skin-Inspired Multifunctional Autonomic-Intrinsic Conductive Self-Healing Hydrogels with Pressure Sensitivity, Stretchability, and 3D Printability. *Adv. Mater.* **2017**, *29*, 1700533.
(30) Jiang, P.; Ji, Z.; Zhang, X.; Liu, Z.; Wang, X. Recent Advances in Direct Ink Writing of Electronic Components and Functional Devices. *Prog. Addit. Manuf.* **2018**, *3*, 65−86.
(31) Rau, D. A.; Forgiarini, M.; Williams, C. B. Hybridizing Direct Ink Write and Mask-Projection Vat Photopolymerization to Enable Additive Manufacturing of High Viscosity Photopolymer Resins. *Addit. Manuf.* **2021**, *42*, 101996.
(32) Cheng, Y.; Chan, K. H.; Wang, X.-Q.; Ding, T.; Li, T.; Lu, X.; Ho, G. W. Direct-Ink-Write 3D Printing of Hydrogels into Biomimetic Soft Robots. *ACS Nano* **2019**, *13*, 13176−13184.
(33) Zhang, A.; Wang, F.; Chen, L.; Wei, X.; Xue, M.; Yang, F.; Jiang, S. 3D Printing Hydrogels for Actuators: A Review. *Chin. Chem. Lett.* **2021**, *32*, 2923−2932.
(34) Ng, W. L.; Lee, J. M.; Zhou, M.; Chen, Y.-W.; Lee, K.-X. A.; Yeong, W. Y.; Shen, Y.-F. Vat Polymerization-Based Bioprinting—Process, Materials, Applications and Regulatory Challenges. *Biofabrication* **2020**, *12*, 022001.
(35) Szymczyk-Ziółkowska, P.; Łabowska, M. B.; Detyna, J.; Michalak, I.; Gruber, P. A Review of Fabrication Polymer Scaffolds for Biomedical Applications Using Additive Manufacturing Techniques. *Biocybern. Biomed. Eng.* **2020**, *40*, 624−638.
(36) Caprioli, M.; Roppolo, I.; Chiappone, A.; Larush, L.; Pirri, C. F.; Magdassi, S. 3D-Printed Self-Healing Hydrogels via Digital Light Processing. *Nat. Commun.* **2021**, *12*, 2462.
(37) Wei, Z.; He, J.; Liang, T.; Oh, H.; Athas, J.; Tong, Z.; Wang, C.; Nie, Z. Autonomous Self-Healing of Poly(Acrylic Acid) Hydrogels Induced by the Migration of Ferric Ions. *Polym. Chem.* **2013**, *4*, 4601−4605.
(38) Wang, Z.; Ren, Y.; Zhu, Y.; Hao, L.; Chen, Y.; An, G.; Wu, H.; Shi, X.; Mao, C. A Rapidly Self-Healing Host−Guest Supramolecular Hydrogel with High Mechanical Strength and Excellent Biocompatibility. *Angew. Chem., Int. Ed.* **2018**, *57*, 9008−9012.
(39) Zhang, H.; Xia, H.; Zhao, Y. Poly(Vinyl Alcohol) Hydrogel Can Autonomously Self-Heal. *ACS Macro Lett.* **2012**, *1*, 1233−1236.
(40) Janusziewicz, R.; Tumbleston, J. R.; Quintanilla, A. L.; Mecham, S. J.; DeSimone, J. M. Layerless Fabrication with Continuous Liquid Interface Production. *Proc. Natl. Acad. Sci. U. S. A.* **2016**, *113*, 11703−11708.
(41) Tumbleston, J. R.; Shirvanyants, D.; Ermoshkin, N.; Janusziewicz, R.; Johnson, A. R.; Kelly, D.; Chen, K.; Pinschmidt, R.; Rolland, J. P.; Ermoshkin, A.; Samulski, E. T.; DeSimone, J. M. Continuous Liquid Interface Production of 3D Objects. *Science* **2015**, *347*, 1349−1352.
(42) Mao, J.; Zhao, C.; Li, Y.; Xiang, D.; Wang, Z. Highly Stretchable, Self-Healing, and Strain-Sensitive Based on Double-Crosslinked Nanocomposite Hydrogel. *Compos. Commun.* **2020**, *17*, 22−27.
(43) Abderrazak, H.; Dachraoui, M.; Lendl, B. A Novel Flow Injection Procedure for Determination of Phosphate in Industrial Raw Phosphoric Acid. *Analyst* **2000**, *125*, 1211−1213.
(44) Anjum, S.; Gurave, P.; Badiger, M. V.; Torris, A.; Tiwari, N.; Gupta, B. Design and Development of Trivalent Aluminum Ions Induced Self-Healing Polyacrylic Acid Novel Hydrogels. *Polymer* **2017**, *126*, 196−205.
(45) Zhao, M.; Tang, Z.; Zhang, X.; Li, Z.; Xiao, H.; Zhang, M.; Liu, K.; Ni, Y.; Huang, L.; Chen, L.; Wu, H. A Self-Healing, Stretchable, and Conductive Poly(N-Vinylpyrrolidone)/Gallic Acid Composite Hydrogel Formed via Hydrogen Bonding for Wearable Electronic Sensors. *Compos. Sci. Technol.* **2020**, *198*, 108294.
(46) Gong, Z.; Zhang, G.; Zeng, X.; Li, J.; Li, G.; Huang, W.; Sun, R.; Wong, C. High-Strength, Tough, Fatigue Resistant, and Self-Healing Hydrogel Based on Dual Physically Cross-Linked Network. *ACS Appl. Mater. Interfaces* **2016**, *8*, 24030−24037.
(47) Song, K.; Zhu, W.; Li, X.; Yu, Z. A Novel Mechanical Robust, Self-Healing and Shape Memory Hydrogel Based on PVA Reinforced by Cellulose Nanocrystal. *Mater. Lett.* **2020**, *260*, 126884.
(48) Zhu, K.; Song, Q.; Chen, H.; Hu, P. Thermally Assisted Self-Healing Polyurethane Containing Carboxyl Groups. *J. Appl. Polym. Sci.* **2018**, *135*, 45929.
(49) Liu, S.; Wang, W.; Xu, W.; Liu, L.; Zhang, W.; Song, K.; Chen, X. Continuous Three-Dimensional Printing of Architected Piezoelectric Sensors in Minutes. *Research* **2022**, *2022*, 9790307.
(50) Zhang, T.; Zuo, T.; Hu, D.; Chang, C. Dual Physically Cross-Linked Nanocomposite Hydrogels Reinforced by Tunicate Cellulose Nanocrystals with High Toughness and Good Self-Recoverability. *ACS Appl. Mater. Interfaces* **2017**, *9*, 24230−24237.
(51) Fu, B.; Cheng, B.; Bao, X.; Wang, Z.; Shangguan, Y.; Hu, Q. Self-Healing and Conductivity of Chitosan-Based Hydrogels Formed by the Migration of Ferric Ions. *J. Appl. Polym. Sci.* **2019**, *136*, 47885.
(52) Das, S.; Martin, P.; Vasilyev, G.; Nandi, R.; Amdursky, N.; Zussman, E. Processable, Ion-Conducting Hydrogel for Flexible Electronic Devices with Self-Healing Capability. *Macromolecules* **2020**, *53*, 11130−11141.
(53) Zhang, X.; Cai, J.; Liu, W.; Liu, W.; Qiu, X. Synthesis of Strong and Highly Stretchable, Electrically Conductive Hydrogel with Multiple Stimuli Responsive Shape Memory Behavior. *Polymer* **2020**, *188*, 122147.
(54) Yuk, H.; Zhang, T.; Parada, G. A.; Liu, X.; Zhao, X. Skin-Inspired Hydrogel−Elastomer Hybrids with Robust Interfaces and Functional Microstructures. *Nat. Commun.* **2016**, *7*, 12028.
(55) Ge, Q.; Chen, Z.; Cheng, J.; Zhang, B.; Zhang, Y.-F.; Li, H.; He, X.; Yuan, C.; Liu, J.; Magdassi, S.; Qu, S. 3D Printing of Highly Stretchable Hydrogel with Diverse UV Curable Polymers. *Sci. Adv.* **2021**, *7*, eaba4261.
(56) Trieu, H.; Qutubuddin, S. Poly(Vinyl Alcohol) Hydrogels: 2. Effects of Processing Parameters on Structure and Properties. *Polymer* **1995**, *36*, 2531−2539.
(57) Gorga, R. E.; Cohen, R. E. Toughness Enhancements in Poly(Methyl Methacrylate) by Addition of Oriented Multiwall Carbon Nanotubes. *J. Polym. Sci., Part B: Polym. Phys.* **2004**, *42*, 2690−2702.
(58) Kim, S.; Lim, H.; Kim, S.; Lee, D. Y. Effect of PVA Concentration on Strength and Cell Growth Behavior of PVA/Gelatin Hydrogels for Wound Dressing. *J. Biomed. Eng. Res.* **2020**, *41*, 1−7.
(59) Sun, J.-Y.; Zhao, X.; Illeperuma, W. R. K.; Chaudhuri, O.; Oh, K. H.; Mooney, D. J.; Vlassak, J. J.; Suo, Z. Highly Stretchable and Tough Hydrogels. *Nature* **2012**, *489*, 133−136.
(60) Ware, H. O. T.; Farsheed, A. C.; Akar, B.; Duan, C.; Chen, X.; Ameer, G.; Sun, C. High-Speed on-Demand 3D Printed Bioresorbable Vascular Scaffolds. *Mater. Today Chem.* **2018**, *7*, 25−34.
(61) Sun, C.; Fang, N.; Wu, D. M.; Zhang, X. Projection Micro-Stereolithography Using Digital Micro-Mirror Dynamic Mask. *Sens. Actuators Phys.* **2005**, *121*, 113−120.
(62) Chen, X.; Liu, W.; Dong, B.; Lee, J.; Ware, H. O. T.; Zhang, H. F.; Sun, C. High-Speed 3D Printing of Millimeter-Size Customized

Aspheric Imaging Lenses with Sub 7 Nm Surface Roughness. *Adv. Mater.* **2018**, *30*, 1705683.
(63) Tuncaboylu, D. C.; Argun, A.; Sahin, M.; Sari, M.; Okay, O. Structure Optimization of Self-Healing Hydrogels Formed via Hydrophobic Interactions. *Polymer* **2012**, *53*, 5513−5522.
(64) Guan, Q.; Lin, G.; Gong, Y.; Wang, J.; Tan, W.; Bao, D.; Liu, Y.; You, Z.; Sun, X.; Wen, Z.; Pan, Y. Highly Efficient Self-Healable and Dual Responsive Hydrogel-Based Deformable Triboelectric Nanogenerators for Wearable Electronics. *J. Mater. Chem. A* **2019**, *7*, 13948−13955.
(65) Gyarmati, B.; Szilágyi, B. Á.; Szilágyi, A. Reversible Interactions in Self-Healing and Shape Memory Hydrogels. *Eur. Polym. J.* **2017**, *93*, 642−669.
(66) Sanders, P.; Young, A. J.; Qin, Y.; Fancey, K. S.; Reithofer, M. R.; Guillet-Nicolas, R.; Kleitz, F.; Pamme, N.; Chin, J. M. Stereolithographic 3D Printing of Extrinsically Self-Healing Composites. *Sci. Rep.* **2019**, *9*, 388.
(67) Cai, L.; Chen, G.; Su, B.; He, M. 3D Printing of Ultra-Tough, Self-Healing Transparent Conductive Elastomeric Sensors. *Chem. Eng. J.* **2021**, *426*, 130545.
(68) Bilodeau, R. A.; Kramer, R. K. Self-Healing and Damage Resilience for Soft Robotics: A Review. *Front. Robot. AI* **2017**, *4*, DOI: 10.3389/frobt.2017.00048.
(69) Roels, E.; Terryn, S.; Iida, F.; Bosman, A. W.; Norvez, S.; Clemens, F.; Van Assche, G.; Vanderborght, B.; Brancart, J. Processing of Self-Healing Polymers for Soft Robotics. *Adv. Mater.* **2022**, *34*, 2104798.
(70) Zhou, Y.; Wan, C.; Yang, Y.; Yang, H.; Wang, S.; Dai, Z.; Ji, K.; Jiang, H.; Chen, X.; Long, Y. Highly Stretchable, Elastic, and Ionic Conductive Hydrogel for Artificial Soft Electronics. *Adv. Funct. Mater.* **2019**, *29*, 1806220.
(71) Kong, W.; Wang, C.; Jia, C.; Kuang, Y.; Pastel, G.; Chen, C.; Chen, G.; He, S.; Huang, H.; Zhang, J.; Wang, S.; Hu, L. Muscle-Inspired Highly Anisotropic, Strong, Ion-Conductive Hydrogels. *Adv. Mater.* **2018**, *30*, 1801934.
(72) Li, L.; Hsieh, Y.-L. Ultra-Fine Polyelectrolyte Fibers from Electrospinning of Poly(Acrylic Acid). *Polymer* **2005**, *46*, 5133−5139.
(73) Alipoori, S.; Mazinani, S.; Aboutalebi, S. H.; Sharif, F. Review of PVA-Based Gel Polymer Electrolytes in Flexible Solid-State Supercapacitors: Opportunities and Challenges. *J. Energy Storage* **2020**, *27*, 101072.
(74) Tang, L.; Wu, S.; Qu, J.; Gong, L.; Tang, J. A Review of Conductive Hydrogel Used in Flexible Strain Sensor. *Materials* **2020**, *13*, 3947.
(75) Tee, B. C.-K.; Wang, C.; Allen, R.; Bao, Z. An Electrically and Mechanically Self-Healing Composite with Pressure- and Flexion-Sensitive Properties for Electronic Skin Applications. *Nat. Nanotechnol.* **2012**, *7*, 825−832.
(76) Choi, M. Y.; Chan, C. K. The Effects of Organic Species on the Hygroscopic Behaviors of Inorganic Aerosols. *Environ. Sci. Technol.* **2002**, *36*, 2422−2428.

https://doi.org/10.1021/acsmaterialslett.3c00439
ACS Materials Lett. 2023, 5, 1727−1737